ACS OMEGA

Open Access

http://pubs.acs.org/journal/acsodf

Article

Synthesis and Antioxidant Studies of 2,4-Dioxothiazolidine-5-acetic Acid Based Organic Salts: SC-XRD and DFT Approach

Syed Muddassir Ali Mashhadi, Moazzam H. Bhatti,* Erum Jabeen, Uzma Yunus, Muhammad Ashfaq, Mahjbeen Akhtar, Muhammad Nawaz Tahir, Saad M. Alshehri, Sarfraz Ahmed, and Suvash Chandra Ojha*

Cite This: *ACS Omega* 2023, 8, 30186−30198

Read Online

ACCESS | Metrics & More | Article Recommendations | Supporting Information

ABSTRACT: In the current study, two organic salts (**1** and **2**) are synthesized, and then crystalline structures are characterized by FTIR, UV spectroscopy, and X-ray crystallographic studies. The organic salts **1** and **2** are optimized at the M06/6-311G(*d*,*p*)level of theory and further utilized for analysis of natural bond orbitals (NBOs), natural population, frontier molecular orbitals (FMOs), and global reactivity parameters, which confirmed the stability of the studied compounds and charge transfer phenomenon in the studied compounds. The studies further revealed that **1** and **2** are more stable than **3**. The lowest energy merged monomer−coformer conformations were docked as flexible ligands with rigid fungal proteins and DNA receptors. The stagnant binding of the monomer through two H bonds with protein was observed for ligands **1** and **3** while different pattern was found with **2**. The coformers formed a single H bond with the active site in **2** and **3** and a single pi−arene H interaction in **1**. The two-point ligand−receptor interactions hooked the monomer between DNA base pairs for partial intercalation; pi stacking with additive hydrogen bonding with the base pair led to a strong benzimidazole interaction in **1** and **2**, whereas ethylene diamine formed weak H bonding. Thus, the molecular docking predicted that the coformer exhibited DNA intercalation reinforced by its salt formation with benzimidazole **1** and methyl benzimidazole **2**. Antioxidant studies depicted that **3** has a higher IC_{50} value than that of 2,4-D and also the largest value among the studied compounds, whereas **2** showed the lowest value among the studied compounds.

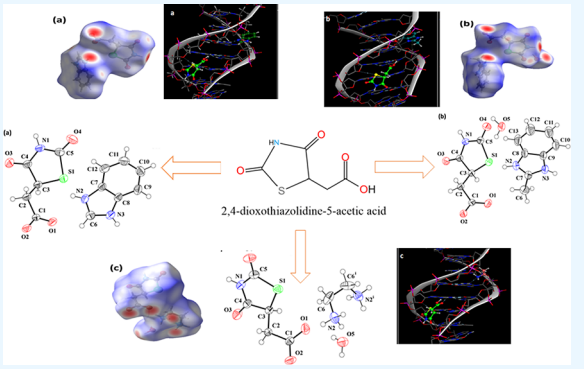

INTRODUCTION

Multicomponent crystals[1,2] like salts are important in designing solid forms in the pharmaceutical industry. Different solid forms display distinct physicochemical properties like bioavailability, stability, flowability, and manufacturability.[3] About half of the marketed drugs are in salt form with stoichiometric anionic and cationic ratio. Normally, higher bioavailability is associated with salt forms,[4] and for complementary ions, a pK_a difference of ≥3 is expected for formation of salts.[5,6] Pharmaceutical organic salt[7−9] is an important solid-state form of drugs having impacts during the drug development process. Heterocyclic aromatic compounds are important pharmacophores due to their promising applications in medicine. Improved bioavailability and solubility profile can be achieved by selection of salt formers, which makes salt selection a multidimensional approach.

The 4-thiazolidinone core represents one of the fortunate design fragments widely utilized as a promising "building block" in modern medicinal chemistry for the rational drug development.[10] 4-Thiazolidinone-based compounds are characterized by various effective biological activities such as anti-inflammatory, analgesic,[11] trypanocidal,[12] anticonvulsant, antiviral,[13] antifungal, antibacterial,[14] anticancer[15] etc. Besides, benzimidazole is a dicyclic organic compound having two nitrogen atoms at the adjoining point attached with a benzene ring. Benzimidazole is a heterocyclic aromatic compound that is also considered as a bioactive compound having a number of biological activities like antiparasitic, antimalarial,[16] antihypertensive, etc. Currently, a variety of drugs containing benzimidazole are available in the market named as cyclobendazole, ridinalazon, thiabendazole, mebendazole, and albendazole.

2,4-Dioxothiazolidine-5-acetic acid (Figure S1) is a thiazolidine derivative containing carbonyl groups, and the substituent leads to the distinction in the structure and properties that have been revealed by structure−activity relationship (SAR) studies.

Received: April 27, 2023
Accepted: July 28, 2023
Published: August 7, 2023

Thiazolidine derivatives are a well-known group of compounds with a wide spectrum of pharmacological activities[17] as shown in Figure S2.

The presence of a 2,4-dioxothiazolidine ring has also been reported in anticonvulsant drugs used for the treatment of diabetes. Several heterocyclic compounds have been observed to have a significant role in the chemotherapy of malignancy.[18] Although 2,4-dioxothiazolidines have been reported to be a potential platform because they are known to stimulate the PPARγ[19] receptor, they also have multiple PPARγ independent effects, and the dose required for anticancer activity of 2,4-dioxothiazolidines is significantly lower than that required for hypoglycemic activity.

In addition to the above-mentioned most suffered diseases, 2,4-dioxothiazolidine also shows an extensive spectrum of pharmacological and anti-inflammatory activities and is used for the treatment of multiple neurological diseases like Parkinson's and Alzheimer's.[20] Furthermore, the reports also suggest it to be antitubercular, antidepressant, and leishmanicidal.

Molecular docking has been studied as an initial screener for drug designing as it defines the interactions of ligands with DNA and proteins.[21] Drugs targeting a single biological target can interfere with other targets too. So the recent advances in molecular docking suggest multitarget docking to elaborate the binding of pharmaceutically active molecules with different macromolecules to obtain an insight into their specificity and pharmacokinetics.[22] So here, we are predicting multiprotein target screening and then presenting the most stable binding in detail.

In the present work, the synthesis and characterization of **1**, **2**, and **3** with medicinal importance are reported. Structural characterization is performed by IR, DSC, and single-crystal XRD analysis. Antioxidant and docking studies are performed to optimize biological activities. Computational studies of **1** and **2** employing DFT-based calculations are performed to evaluate the potential optical properties of synthesized materials by optimizing the natural bond orbitals (NBOs), vibrational analysis, frontier molecular orbitals (FMOs), global reactivity parameters (GRPs), and molecular electrostatic potential (MEP) surfaces.

RESULTS AND DISCUSSION

The supramolecular interactions of 2,4-dioxothiazolidine-5-acetic acid and coformers resulted in organic salts that are analyzed by various characterization techniques. Table 1 lists the physical properties of studied crystals. UV−vis studies are explained in the Supporting Information (Tables S1a, S1b, and S1c).

IR Spectroscopic Findings. IR analysis showed the formation of products by producing distinct peaks in spectra, and the results are arranged in Table 2 and Tables S18 and S19. The IR spectra are shown in Figures S4−S6. The carbonyl group belonging to the amide functional group was absorbed at 1689, 1680, and 1660, respectively, for **1**, **2**, and **3**. The carbonyl group attached to sulfur showed absorption at 1736, 1727, and 1748 for **1**−**3**, respectively. The carboxyl hydroxyl group in **1** and **3** showed peaks at 3138 and 3048, respectively. Additionally, DFT calculations (vibrational frequencies and Raman vibrational frequencies) were also performed for compounds **1** and **2** (Tables S18−S20). A comparison between DFT and experimental values is developed, and harmony is seen as illustrated in Table 2.

Table 1. Physical Properties of Crystalline Products

codes	empirical formula	molecular weight (g/mol)	physical appearance	melting point (°C)
2,4-D	$C_5H_5NSO_4$	175		167−169 °C
1	$C_{12}H_{11}N_3O_4S$	293.30	light yellow prism	192
2	$C_{13}H_{15}N_3O_5$	325.34	colorless prism	222
3	$C_6H_{11}N_2O_5S$	223.23	colorless prism	130

Table 2. Functional Group Identification Using IR Results of 1−3

comp.	functional group	FTIR frequency (cm^{-1}) exp.	vibrational frequency (cm^{-1})	Raman vibrational frequencies (cm^{-1})
1	−OH (carboxyl)	3138.00	3102	3039
	−C═N	1314.24	1332	1326
	C═O (S−C═O)	1736.89	1854	1845
2	C═O (amide)	1680.24	1680	1620
3	−OH (carboxyl)	3046.46		
	C═O (amide)	1660.57		
	N−H	3139.73		
	C═O (S−C═O)	1748.33		
	C−H	2986.71		
	$-CH_2-$ bending	1445.18		
	C−N	1065.23		

Single-Crystal XRD Results. The salt crystal strctures **1** (Figure 1a), **2** (Figure 1b), and **3** (Figure 1c) have the same anion named as 2-(2,4-dioxothiazolidin-5-yl)acetate but have a different cation, and crystal parameters are arranged in Table 3. The crystal structure of salt **1** is anhydrous, whereas salts **2** and **3** are hydrated. The cation is 1*H*-benzo[*d*]imidazol-3-ium, 2-methyl-1*H*-benzo[*d*]imidazol-3-ium, and ethane-1,2-diaminium in salts **1**, **2**, and **3**, respectively. In the anion, the acetate group A (C1/C2/O1/O2) and thiazolidine-2,4-dione ring B (C3-C5/N1/O3/O4/S1) are planar with a root mean square (r.m.s.) deviation of 0.0039 and 0.0031 Å, respectively, in salt **1**; 0.0018 and 0.0136 Å, respectively, in salt **2**; and 0.0048 and 0.0145 Å, respectively, in salt **3**. The dihedral angle A/B is 52.03 (4), 58.67 (4), and 47.23 (4)° in salts **1**, **2**, and **3**, respectively. In salt **1**, the 1*H*-benzo[*d*]imidazol-3-ium cation is planar with an r.m.s deviation of 0.0183 Å, whereas in salt **2**, the 2-methyl-1*H*-benzo[*d*]imidazol-3-ium cation is planar with an r.m.s. deviation of 0.0037 Å. The anions of salt **1** are interlinked with each other through N−H···O bonding.

The cation and anion are inlinked through N−H···O and C−H···O bonding (Figure 2, Table S17). The further stablization of the crystal packing in salt **1** is due to offset $\pi\cdots\pi$ stacking interactions with intercentroid separation range from 3.4725 (9) to 4.3705 (9) Å. The anions of **2** are interlinked with each other through N−H···O bonding as well as through C−H···O bonding. The cations and anions are inlinked through C−H···O bonding.

https://doi.org/10.1021/acsomega.3c02895
ACS Omega 2023, 8, 30186−30198

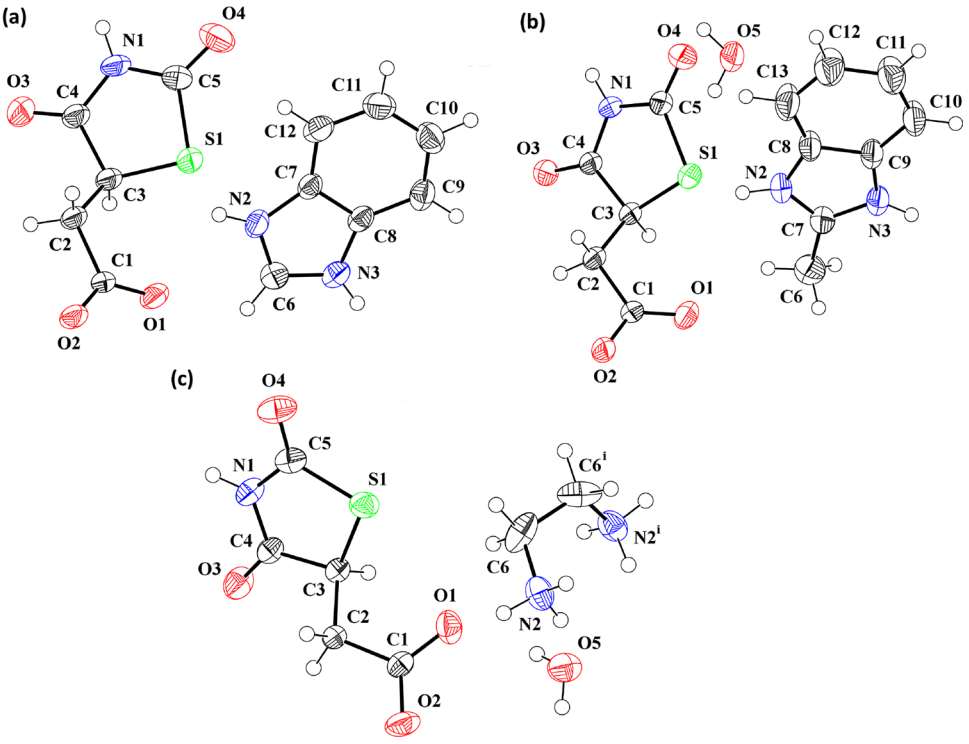

Figure 1. ORTEP diagrams drawn at a probability level of 50%. H-atoms are shown by small circles of arbitrary radii. Crystal structures of **1**, **2**, and **3** are represented as a, b, and c, respectively.

The water molecule plays an important role as it is connected with cations and anions through O−H···O bonding (Figure 3, Table S17). The further stablization of the crystal packing of salt **2** is due to C−O···π interaction (Table 2) and the offset π···π stacking interactions with intercentroid separation range from 3.7016 (12) to 4.3603 (11) Å.

Like in salt **2**, the anions of salt **3** are interlinked with each other through N−H···O bonding as well as through C−H···O bonding, and the cations and anions are inlinked through C−H···O bonding. The water is interlinked with anions through O−H···O bonding, whereas it is interlinked with cations through N−H···O bonding. The further stablization of the crystal packing of salt **3** is due to C−O···π interaction (Figure 4, Table S17) and the offset π···π stacking interactions with an intercentroid separation distance of 3.9872(8) Å. The cations are not directly interlinked through any H-bonding in salts **1**, **2**, and **3**.

TGA-DTA/DSC Results. DSC results (Figures S7−S9) show the distinct melting point and decomposition in a single stage (Table 4), and the results are arranged in Table 6. The DSC thermograms are shown in Figures S7−S9. Endothermic peaks for **1**−**3** were noted to be at 191.42, 221.94, and 130.58 °C.

Antioxidant (DPPH) Assay. Antioxidant studies are shown in Table 5, which depicts that compound **3** shows the largest IC_{50} value and **2** shows the lowest among the studied compounds.

Hirshfeld Surface Analysis. Hirshfeld surface (HS) inquiry is a wonderful sort of analysis to investigate the intermolecular interactions of any kind in single crystals by employing CrystalExplorer 21.5.[23] The Hirshfeld surface can be constructed by employing several properties like dnorm, shape index, curvedness, fragment patches, etc. We are going to explore the HS over dnorm and shape index. HS plotted over dnorm provides a direct insight of the H-bonding interactions in single crystals by using three colors (red, white, and blue).[24] The short contacts are displayed by red spots on the HS. Figure 5a−c shows HS over dnorm for **1**, **2**, and **3**, respectively. The atoms involved in H-bonding interactions are shown by red spots on the HS for **1**, **2**, and **3**. HS over shape index provides information about the interaction weaker than H-bonding, i.e., π···π stacking interactions.[25] Figure 5d,e shows the HS plotted over shape index for **1**, **2**, and **3**, respectively. For salts **1**−**3**, the constructive red and blue regions on the HS of triangular shape are the indication of π···π stacking interactions. The 2D fingerprint analysis is explained in the Supporting Information.

Geometrical Parameters. The geometrical parameters for **2** such as the bond lengths for S-C atoms were calculated through DFT, and the values were found to be 1.832 and 1.780 Å for S1-C9 and S1-C11, respectively, whereas through XRD, the values were obtained to be 1.813 and 1.768 Å, respectively. On the other hand, for **1**, the lengths between sulfur and carbon atoms were found to be 1.79 and 1.211 Å (DFT) for S1-C9 and S1-C11, respectively, whereas through XRD, the values were 1.768 and 1.240 Å, respectively. For **2**, the bond lengths between oxygen and carbon atoms were found to be 1.322, 1.204, 1.199, and 1.202 Å for O2-C7, O3-C7, O4-C10, and O5-C11, respectively (DFT), whereas through XRD, the values were 1.235, 1.264, 1.220, and 1.205 Å, respectively. For **1**, the calculated bond lengths between oxygen and carbon atoms were found to be 1.312, 1.200, 1.193, and 1.376 Å for O2-C7, O3-C7, O4-C10 and, O5-C11, respectively, whereas the values were obtained to be 1.263, 1.212, 1.207, and 1.367 Å, respectively (XRD). These detailed geometrical parameters were tabulated in the supporting data (Tables S2 and S3). The values of C-C bond length for C8-C9 and C9-C10 in compound **1** were observed to be 1.519 and 1.516 Å,

https://doi.org/10.1021/acsomega.3c02895
ACS Omega 2023, 8, 30186−30198

Table 3. Single-Crystal XRD Results of 1−3

crystal data	1	2	3
CCDC	2208506	2208507	2208508
chemical formula	$C_{12}H_{11}N_3O_4S$	$C_{13}H_{15}N_3O_5S$	$C_6H_{11}N_2O_5S$
M_r	293.30	325.34	223.23
crystal system, space group	triclinic, $P\bar{1}$	triclinic, $P\bar{1}$	monoclinic, $C2/c$
temperature (K)	296	296	296
a, b, c (Å)	8.3530 (6), 8.8839 (6), 9.2360 (7)	8.2040 (8), 8.2497 (9), 11.7274 (11)	19.061 (1), 14.0218 (9), 7.1586 (4)
α, β, γ (°)	81.315 (2), 79.350 (2), 77.983 (2)	105.971 (2), 100.746 (3), 91.222 (2)	90, 93.818 (2), 90
V (Å^3)	654.28 (8)	747.48 (13)	1909.03 (19)
Z	2	2	8
density (calculated)	1.489 Mg/m^3	1.446 Mg/m^3	1.553 Mg/m^3
$F(000)$	304	340	936
radiation type	Mo Kα	Mo Kα	Mo Kα
wavelength (λ)	0.71073 Å	0.71073 Å	0.71073 Å
μ (mm^{-1})	0.265	0.244	0.339
crystal shape	prism	prism	prism
crystal color	light yellow	colorless	colorless
crystal size (mm)	0.42 × 0.36 × 0.32	0.44 × 0.34 × 0.30	0.45 × 0.38 × 0.35
data collection			
absorption correction	multiscan (SADABS; Bruker, 2007)	multiscan (SADABS; Bruker, 2007)	multiscan (SADABS; Bruker, 2007)
no. of measured, independent and observed [$I > 2$ s(I)] reflections	7469, 2809, 2520	9519, 3522, 3145	4935, 2034, 1854
R_{int}	0.035	0.031	0.031
theta range for data collection	2.525 to 27.081°	2.576 to 27.886°	3.435 to 27.095°
index ranges	$-10 \le h \le 10$, $-11 \le k \le 11$, $-11 \le l \le 11$	$-10 \le h \le 10$, $-10 \le k \le 10$, $-15 \le l \le 11$	$-24 \le h \le 22$, $-14 \le k \le 17$, $-8 \le l \le 9$
$(\sin \theta/\lambda)_{max}$ (Å^{-1})	0.641	0.658	0.641
refinement			
$R[F^2 > 2\sigma(F^2)]$, $wR(F^2)$, S	0.039, 0.105, 1.05	0.039, 0.113, 1.05	0.032, 0.089, 1.06
no. of reflections	2809	3522	2034
no. of parameters	181	208	136
H-atom treatment	H-atom parameters constrained	H atoms treated by a mixture of independent and constrained refinement	H atoms treated by a mixture of independent and constrained refinement
$\Delta\rho_{max}$, $\Delta\rho_{min}$ (e Å^{-3})	0.30, −0.22	0.35, −0.22	0.31, −0.21

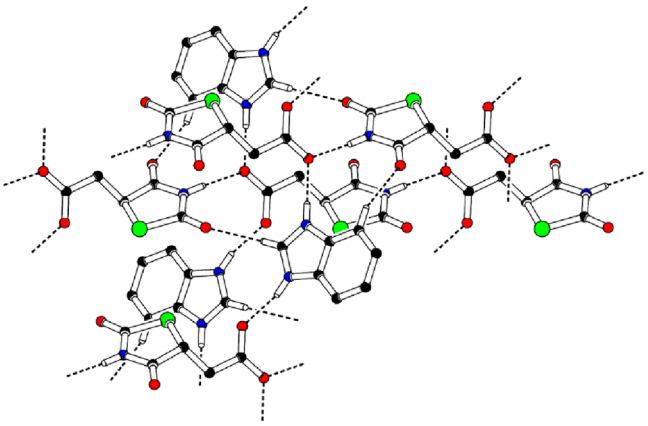

Figure 2. Packing diagram of **1**.

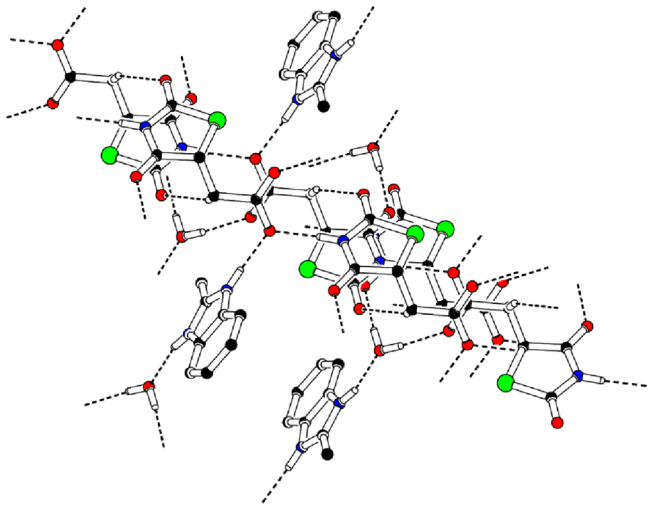

Figure 3. Packing diagram of **2**.

respectively. In compound **2**, the observed bond lengths for C7-C8 and C8-C9 were found to be 1.514 and 1.518 Å, respectively. Thus, these results displayed a good agreement with the value of C-C bond length (1.493 Å) computed in dichloromethane (DCM).. Moreover, the bond angle among carbon atoms in C18-C19-C20 (121.7°) as well as C19-C20-C21 (121.1°) for compound **1** and C15-C16-C17 (121.6°) as well as C16-C17-C18 (121.5°) for compound **2** showed good harmony with the C-C bond angle (121.5°) calculated in DCM.

Additionally, the root mean square error (RMSE) is contemplated as a significant approach to be utilized in structural calculations. So, RMSE has also been computed for

https://doi.org/10.1021/acsomega.3c02895
ACS Omega 2023, 8, 30186−30198

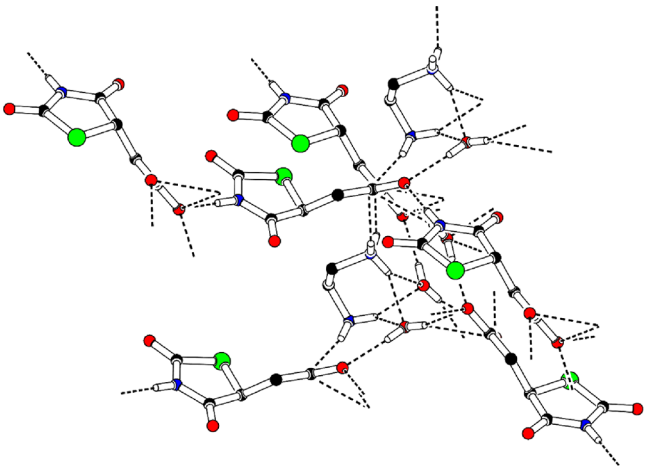

Figure 4. Packing diagram of **3**.

our investigated chromophores (**1** and **2**), and results are tabulated in Table 6. For bond length values of our studied systems, RMSE results were found to be less in magnitude. Meanwhile, greater values of RMSE were observed for bond angles due to higher deviation of bond angles between carbon and oxygen.

Natural Bond Orbital (NBO) Analysis. NBO analysis is an efficient tool that effectively describes the interaction among bonds, intramolecular charge transfers, and several second-order interactions between the filled and the vacant orbitals. It also offers detailed information about intramolecular and intermolecular hydrogen bonding.[26] The second-order Fock matrix was utilized to estimate the donor−acceptor interactions in the NBO basis. For every donor (i) and acceptor (j) with accompanying $i-j$ delocalization, the perturbation stabilization energy $E^{(2)}$ is evaluated by eq 1.[27]

$$E^{(2)} = q_i \frac{(F_{i,j})^2}{\varepsilon_j - \varepsilon_i} \quad (1)$$

In eq 1, $F_{i,j}$ is the off diagonal NBO Fock matrix element, ε_i and ε_j are the diagonal elements, and q_i is the donor orbital occupancy. The most prominent energies of stabilization, which vary among the different orbitals, are shown in Table 7 for **1** and **2**, respectively. The detailed data for the transitions in **1** and **2** are presented in Tables S4 and S5 of the supporting data.

The occurrence of conjugation in investigated compounds can be judged by examining of $\pi \rightarrow \pi^*$ transitions. The most prominent transitions with high stabilization energy observed in our systems were π(C31-C33) → π^*(C27-C29) and π(C25-C26) → π^*(C27-C29) in **2** with 22.46 and 20.33 kJ/mol stabilization energy values and π(C24-C26) → π^*(C20-C22)

Table 5. Antioxidant (DPPH) Assay of Compounds 1−3

DPPH radical scavenging activity (%)	
compounds	IC_{50} value (ppm)
2,4-D	34.13
gallic acid	2.6
1	22.42
2	13.58
3	52.97

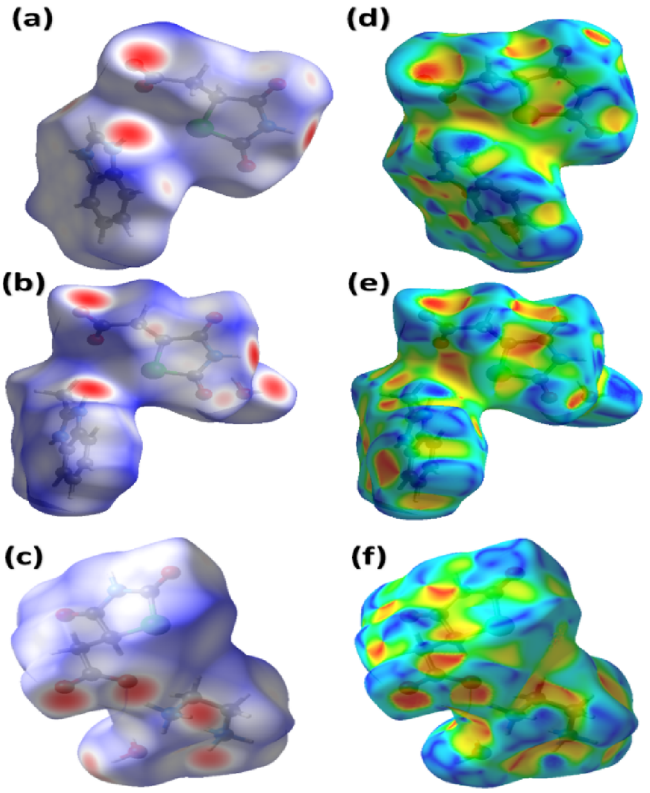

Figure 5. Hirshfeld surface plotted over dnorm for (a) **1** in the range −0.7210 to 1.7517 a.u., (b) **2** in the range −0.7340 to 1.2712 a.u., and (c) **3** in the range −0.6889 to 1.5082 a.u. Hirshfeld surface plotted over shape index in the range −1 to 1 a.u. for (d) **1**, (e) **2**, and (f) **3**.

Table 6. Calculated Error Values for Compounds 1 and 2[a]

derivatives	parameter	MAD	RMSE	MAPE
1	bond length	0.0159	0.0259	1.1923
	bond angle	1.7967	2.4966	1.5588
2	bond length	0.0138	0.0183	1.0044
	bond angle	1.3964	1.8037	1.2205

[a]MAD = mean absolute deviation, RMSE = root mean square error, MAPE = mean absolute percentage error.

Table 4. TGA-DTA/DSC Data of Compounds 1−3

		thermogravimetry			
			weight loss (%)		
compound	endothermic peak (DSC) (°C)	temp. range (°C)	found	calc.	decomposition species
1	191.42	190−800	99	99	salt of 2,4-dioxothiazolidine-5-acetic acid and benzimidazole
2	221.94	129−700	100	100	salt of 2,4-dioxothiazolidine-5-acetic acid and 2-methylbenzimidazole
3	130.58	130−800	99	100	salt of 2,4-dioxothiazolidine-5-acetic acid and ethylene diamine

https://doi.org/10.1021/acsomega.3c02895
ACS Omega 2023, 8, 30186−30198

Table 7. Natural Bond Orbital (NBO) Analysis of 1 and 2 Using M06/6-311G(d,p)

comp.	donor (i)	type	acceptor (j)	type	$E^{(2)}$ [kcal/mol]	$E(j)-E(i)$ (a.u.)	$F(i,j)$ (a.u.)
1	C24-C26	π	C20-C22	π^*	21.88	0.30	0.073
	C18-C19	π	C20-C22	π^*	19.93	0.30	0.070
	C9-H10	σ	S1-C12	σ^*	5.85	0.66	0.055
	O3-H29	σ	C16-N28	σ^*	0.08	1.30	0.009
	O3	LP(2)	O2-C8	π^*	61.01	0.35	0.132
	O5	LP(2)	S1-C15	σ^*	35.29	0.44	0.113
2	C31-C33	π	C27-C29	π^*	22.46	0.29	0.073
	C25-C26	π	C27-C29	π^*	20.33	0.30	0.071
	C9-H10	σ	S1-C12	σ^*	5.94	0.65	0.056
	O3-C8	σ	O2-C8	σ^*	0.51	1.51	0.025
	N6	LP(1)	O5-C15	π^*	56.58	0.30	0.116
	O3	LP(2)	O2-C8	σ^*	31.00	0.68	0.132

and π(C18-C19) → π^*(C20-C22) in **1** with stabilization energies of 21.88 and 19.35 kJ/mol, respectively.

In a similar fashion, the highest $\sigma \rightarrow \sigma^*$ interactions with maximum energies of stabilization could be noticed in σ(C9-H10) → σ^*(S1-C12) with energy of 5.94 kJ/mol in **2** and σ(C9-H10) → σ^*(S1-C12) with a value of 5.85 kJ/mol in **1**. Meanwhile, $\sigma \rightarrow \sigma^*$ transitions with minimum energies of stabilization observed were σ(O3-C8) → σ^*(O2-C8) with energy of 0.51 kJ/mol in **2** and σ(O3-H29) → σ^*(C16-N28) with a value of 0.08 kJ/mol in **1**.

Furthermore, in the case of resonance, some significant transitions were also recorded because of lone pairs LP1(N6) → π^*(O5-C15) and LP2(O3) → σ^*(O2-C8) with values of 56.58 and 31.00 kJ/mol in **2** and LP2(O3) → π^*(O2-C8) and LP2 (O5) → σ^*(S1-C15) with energies of 61.01 and 35.29 kJ/mol in **1**.

From discussion, it is clear that extended conjugation was present in the studied molecules and involved strong intramolecular hyperconjugative interactions that were noticed due to the ICT process in all compounds and led to the stabilization of the abovementioned compounds. Moreover, the presence of extended conjugation and charge shifting phenomena proves the red-shifted behavior of these compounds.

Frontier Molecular Orbitals (FMOs). Not only do frontier molecular orbitals (FMOs) elaborate the optoelectronic properties of organic solar cells (OSCs), but also, the chemical stability of designed systems is construed with this analysis.[28−30] FMO analysis is an imperative tool to assess the probability of charge transfer among designed molecules.[31−34] The frontier molecular orbital diagrams envisioned at the M06/6-311G(d,p) level for all investigated molecules are shown in Figure 6. From FMOs, we can evaluate the distribution pattern of electron density in molecular orbitals. FMOs not only help to elucidate the chemical affinity and interaction of the investigated molecule with other moieties but also help us to decode the reactive sites in any π-electron system.[35−37]

The charge carrier mobility is enhanced in investigated molecules (**2** and **1**) through modification in their moieties, which supported the electronic delocalization in the molecular systems. Therefore, the FMO study is carried out for investigated molecules, and their results are shown in Table S14. Moreover, other results are exhibited in Table S15.

The calculated energies of HOMO of chromophores **1** and **2** were −6.995 and −6.771 eV, respectively. The energies of LUMO of compounds **1** and **2** were −0.818 and −0.932 eV,

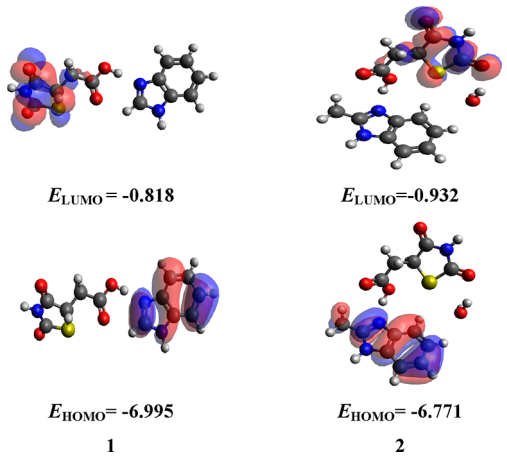

Figure 6. HOMO/LUMO maps of investigated compounds (**1** and **2**).

respectively. ΔE was considered as the most substantial tool to represent the charge transfer as well as optoelectronic properties in molecules. So, the ΔE value for studied compound **1** was 6.177 eV, and for compound **2**, it was 5.839 eV. In an exceptional manner, compound **1** contained the maximum band gap among all studied compounds, *i.e.*, 6.177 eV. Meanwhile, compound **2** showed the minimum energy band gap, *i.e.*, 5.839 eV. In that case, there would be maximum charge transfer from HOMO to LUMO. **2** showed ΔE value smaller than **1** (6.177 eV), which is why it showed a larger ICT than **1**.

Furthermore, the contour sides of the FMOs have also been operated to explain the electronic cloud transference phenomena, as displayed in Figure 6. Moreover, other results are depicted in Figure S3.

Global Reactivity Parameters. HOMO and LUMO energies can be employed to explain the stability of compounds **2** and **1** in terms of GRP descriptors.[38−40] The value of the energy bad gap ($\Delta E = E_{LUMO} - E_{HOMO}$) has an inverse relation with the reactivity and softness of the compound and a direct relation with the stability and hardness of the studied species.[41] The FMO energy band gap ($E_{gap} = E_{LUMO} - E_{HOMO}$) interprets the electron transference properties, reactivity, hardness, and softness of the molecule. A higher value of E_{gap} for molecules expresses greater stability, lower chemical affinity, and more hardness value, which suggest that they may cause confliction to change in electronic arrangement. On the other hand, molecules that possess a lesser band

https://doi.org/10.1021/acsomega.3c02895
ACS Omega 2023, 8, 30186−30198

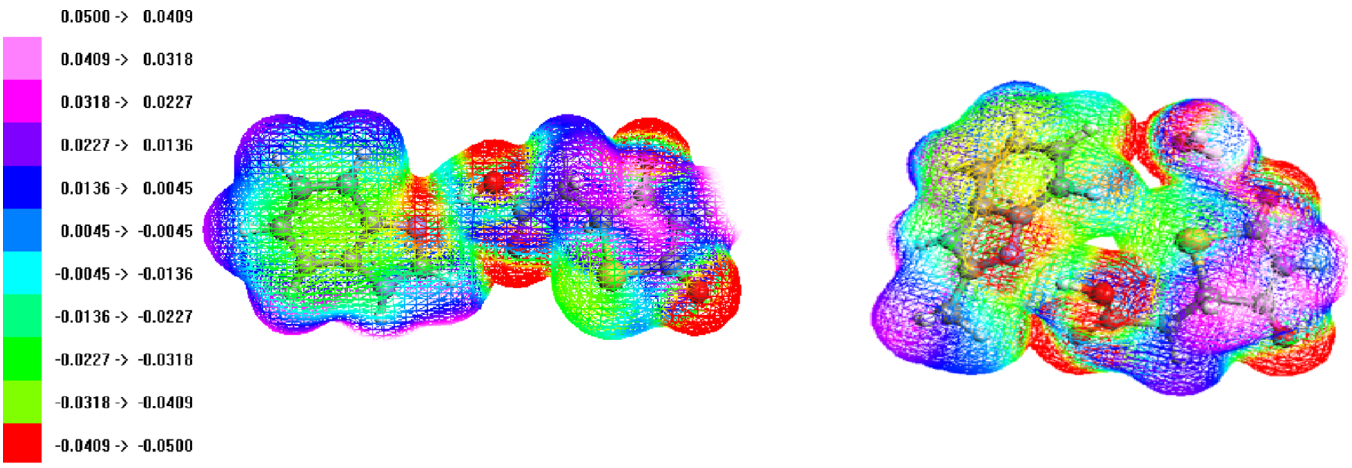

Figure 7. MEP graphs of compounds **1** and **2**.

gap value are observed as soft molecules having high reactivity, less stability, and easy tunability. **1** and **2** showed greater ionization potential as compared to electron affinity given in Table S16.

The values of ionization potential and electron affinity of compound **1** were found to be greater than **2**. The observed chemical hardness values for investigated compounds were greater as compared to softness values. By comparing the results of studied compounds, it was observed that compound **1** had greater hardness and the lowest softness value. This depicts that compound **1** was more stable, less reactive, and harder than **2** (Table S13). Chemical potential provides support to explain the stability and reactivity of compounds **2** and **1** and has a direct association with the stability and an inverse relation to the reactivity of the compounds under examination. Natural population analysis (NPA) (Figure S10) is also performed and is included in the Supporting information. The results of NPA are depicted in Figure S10.

Molecular Electrostatic Potential (MEP). The chemical and physical sides of any system could be explored by the molecular electrostatic potential (MEP) plot. Generally, the MEP plot could be employed to comprehend the plausible nucleophilic or electrophilic attack at suitable sites on chemical structures. The surface of MEP contains several typical colors like green, blue, red, orange, and yellow revealing the magnitude of electrostatic potential. The order of magnitude of electrostatic potential in decreasing order was found to be blue > green > yellow > orange > red. The highlighted segment with red color has a negative potential value, which was supportive for the attack of an electrophile. On the contrary, the nucleophile enticing site by most positive potential could be displayed through blue color. MEP was characterized by using eq 2, and the surface diagrams are displayed in Figure 7. In the present study, the sulfur, nitrogen, and oxygen atoms of investigated compounds containing negative potential might be favorable atoms for the electrophilic attack.

$$V(r) = \sum \left(\frac{Z_A}{R_A} - r \right) - \int p(r') / (r' - r) dr' \quad (2)$$

The MEP was associated with electron density and presented very suitable indices for determining electrophilic and nucleophilic reactions and interaction due to hydrogen bonding.

Molecular Docking. The interactive potencies with fungal immune-protein and DNA were assayed through molecular docking. In the semiflexible multiple receptor model, the rigid default receptors (macromolecule) were docked with the flexible ligand.

The most stable interactions of the compounds with clear acceptor donor interactions were obtained with fungal protein 1OSY (Table 8).

Table 8. Docked Screening of Multitarget Receptors

	docking score for binding with protein			
salts	1OSY (fungal immune protein)	6HNI (bacterial transport protein)[42]	1TD7 (phospholipase A2; proinflammation producing compound)[a43]	6I93 (bacterial oxydoreductase)[44]
1	−4.362	−3.217	−2.41	−4.02
2	−4.112	−3.438	−2.32	−3.99
3	−3.415	−3.832	−2.41	−3.24

[a]Phospholipase A2 (PLA2; EC 3.1.3.4) catalyzes the first step of the production of proinflammatory compounds collectively known as eicosanoids.

The docked conformations of **1** to **3** with the fungal protein (PDB ID: 1OSY) are given in Figure 8 as 3D interactional poses. The binding of merged structures of the salts found different interactional pockets in the protein receptor in the lowest energy conformation as can be seen in Figure 8. This reveals the independent binding behavior of both ions of the

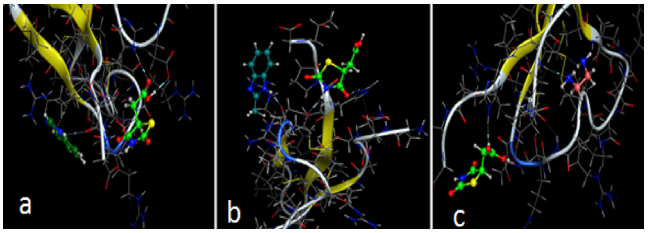

Figure 8. 3D docked poses of (a) **1**, (b) **2**, and (c) **3** with protein (PDB ID: 1OSY).

https://doi.org/10.1021/acsomega.3c02895
ACS Omega 2023, 8, 30186−30198

salt. This is logical as both components of salts interact with protein as separate integrities in the solvent medium. The most stable docked conformations predicted the independent binding patterns for all the studied compounds in protein pockets. The 2,4-dioxothiazolidine-5-acetic acid monomer can develop a two-point interaction with amino acids at the active site. However, the exact binding site of this monomer was influenced by its conformer (Table 9). The benzimidazole conformer and methyl benzimidazole conformers in **1** and **2** were able to develop pi−pi interactions with long-chain amino acids. Both components of salt **3** can bind with this protein through two-point H bonding by the monomer and one-point H bonding by its conformer but at different sites.

Table 9. Molecular Docking Results

	amino acid interactions by		docking score for binding with	
salts	monomers	counter ions	protein	DNA
1	2 points	1 donor + 1 pi−arene	−4.362	−6.338
2	1 donor and 1 acceptor	1 donor	−4.112	−6.129
3		1 acceptor	−3.415	−5.943

Figure 9 corresponds to 2D interactional profiles of salts and reveals side chain donor−acceptor interaction with the protein for the monomer with an acceptor behavior of conformations in **3** and a donor behavior of stable conformation in **1**. In **1**, the interaction is further strengthened by additional arene H interaction. Salt **2** exhibited a different side chain donor−acceptor site in the monomer with the H bond donor behavior of conformer. These observations revealed that monomer interactions with the active site of albumin in docked conformations were independent of their coformers in **1** and **3**. In compounds **1** and **2**, the counter ions exhibited slight interaction with albumin, whereas the counter ion in **2** directly influenced the binding behavior of the monomer.

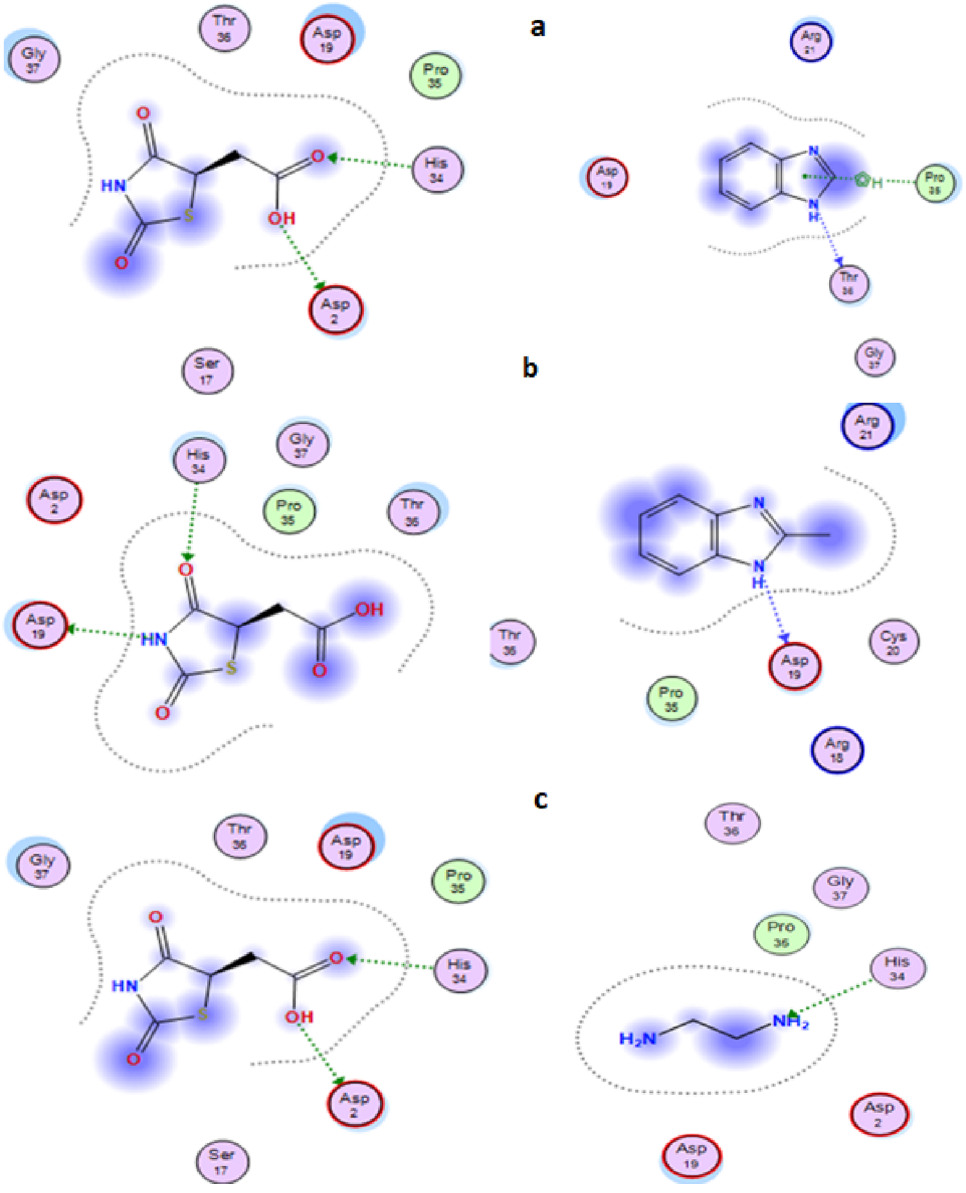

Figure 9. 2D interactional poses of (a) **1**, (b) **2**, and (c) **3** with protein (PDB ID: 1PRB).

https://doi.org/10.1021/acsomega.3c02895
ACS Omega 2023, 8, 30186−30198

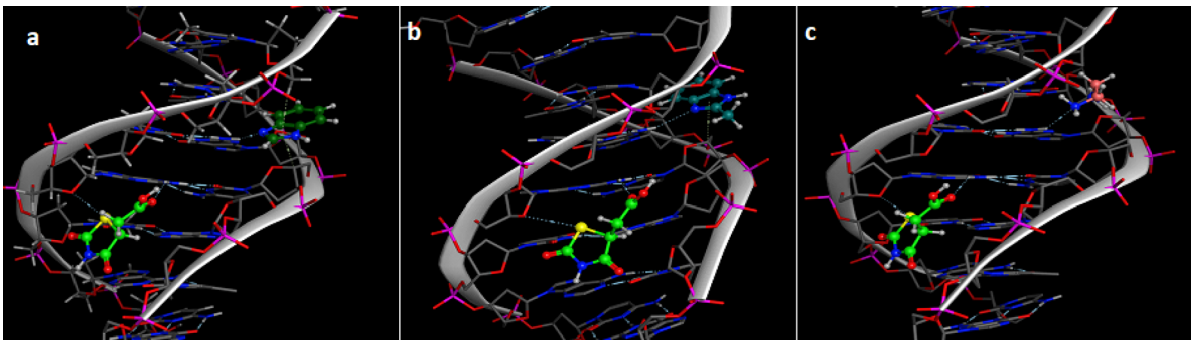

Figure 10. 3D docked conformations of (a) **1**, (b) **2**, and (c) **3** with dsDNA (PDB ID: 1D18).

Scheme 1. Synthesis of 2,4-Dioxothiazolidine-5-acetic Acid

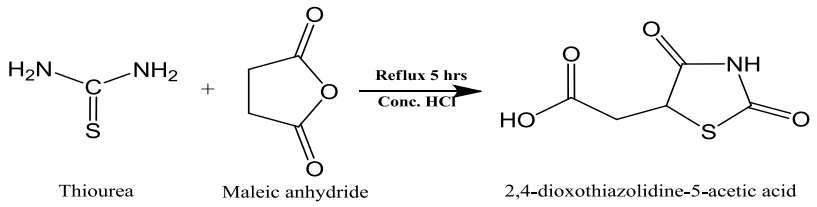

The donor−acceptor potencies of each compound can be related with the DFT computed isodensities of frontier molecular orbitals given in Figure 6 and Figure S3. The HOMO isodensity is spread over benzimidazole and methyl benzimidazole ion, which depicts its involvement in electron pair donation in any ET reaction. The common ion exhibited dual (donor−acceptor) behavior though at different sites depending upon the attached counter ion, which reveals the involvement of LUMO and some donor orbital lower than HOMO. By looking at the isodensities of the underlying orbitals, it can be predicted that the HOMO-2 of **1** and HOMO-1 of **2**, with isodensities at common ion, could be involved in the respective protein binding (Figure 8). The HOMO-1 of **1** having isodensities at the counter ion might be responsible for developing the pi−arene interaction with the protein base pair. So, the combined DFT computed FMO spread and molecular docking results predict protein binding of compounds as depicted in Figures 9 and 10.

The docked conformations of investigated compounds with dsDNA (PDB ID: 1D18) are given in Figure 10, which reveals two-point DNA binding by monomer and conformers in all the studied compounds. The monomer 2,4-dioxothiazolidine-5-acetic acid gets hooked between the DNA base pair and stands through two-point ligand−receptor interactions, whereas the coformer exhibits independent binding patters. The pi stacking with the phosphate backbone with simultaneous hydrogen bonding with the base pair can impart additional strength of interaction with DNA to benzimidazole moiety in **1** and **2** (Figure 10a,b). The ethylene diamine can form weak H bonding with DNA in **3** (Figure 10c). Thus, the DNA interacting power of 2,4-dioxothiazolidine-5-acetic acid can be reinforced by its salt formation with benzimidazole **1** and methyl benzimidazole **2**, as the DNA binding strength was higher from the merged structure than that for their free counterparts. Meanwhile, the monomer's salt with ethylenediamine (**3**) did not interfere with the docking response of the monomer to a greater extent. So, enhanced DNA binding can be predicted for **1** and **2**.

So, on the basis of fungal immune protein and DNA binding potencies, these compounds can be investigated for their antifungal and DNA binding potentials.[45−49]

CONCLUSIONS

Three new salts (**1**−**3**) have been developed by reacting the 2,4-dioxothiazolidine-5-acetic acid with benzimidazole, 2-methylbenzimidazole, and ethylenediamine. Adducts were obtained in 1:1 crystalline forms and analyzed by TGA-DSC, FTIR spectroscopy, UV spectroscopy, and single-crystal XRD studies. The DPPH radical scavenging (antioxidant) studies revealed that the greater the IC_{50} value is, the lower is the antioxidant scavenging activity. DFT calculations of **1** and **2** were accomplished at the M06/6-311G(*d*,*p*) level, and their structures showed good agreement with the experimental results, which confirm the stability of molecules (**1** and **2**). The presence of charge shifting phenomena and extended conjugation proved the red-shifted behavior of these compounds. Compound **2** showed the maximum absorbance in the UV−vis region and gave the highest λ_{max} peak having a value of 568.526 nm. The highest molecular orbital contribution was shown by **2**, whereas the lowest was shown by **1**. Compound **2** (5.839 eV) showed a smaller energy band gap (ΔE) than **1** (6.177 eV); therefore, it showed a larger ICT than **1**. It was observed that compound **1** had greater hardness and the lowest softness value. This depicted that compound **1** was more stable, less reactive, and harder than **2**.

Docking results depicted the interactive potencies with fungal immune-protein and DNA, and the docked conformation of **1** to **3** with fungal protein (PDB ID: 1OSY) reveals the independent binding behavior of structures of the salts with different interactional pockets in the protein receptor. These studies provide motivation for further in vivo and in vitro studies to explore the medicinal and optical implication of synthesized compounds.

EXPERIMENTAL SECTION

Synthesis of 2,4-Dioxothiazolidine-5-acetic Acid. Maleic anhydride and thiourea were mixed with concentrated

https://doi.org/10.1021/acsomega.3c02895
ACS Omega 2023, 8, 30186−30198

Scheme 2. Synthesis of Organic Salts

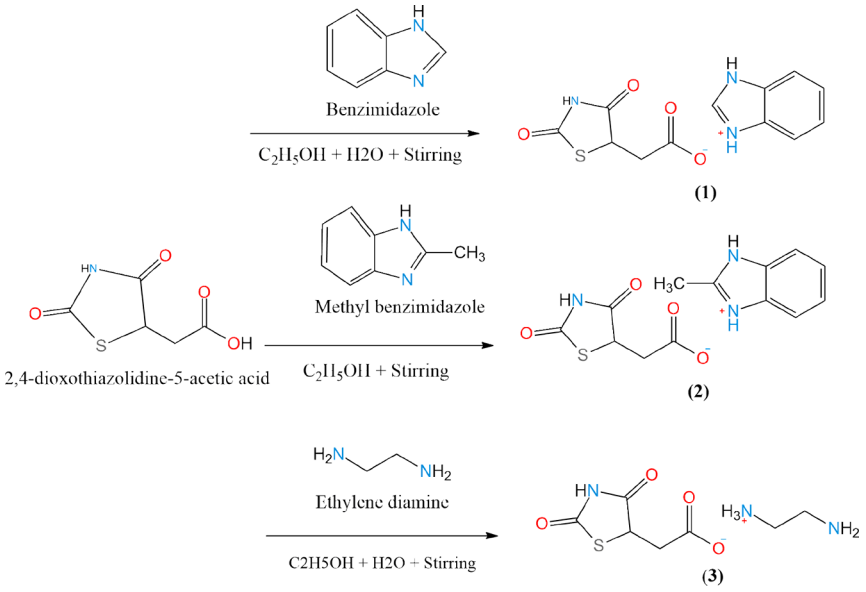

HCl and refluxed in a round-bottom flask for 5 to 7 h to yield (about 75%) 2,4-dioxothiazolidine-5-acetic acid[50] followed by recrystallization in water (Scheme 1 and Table 1).

Synthesis of Organic Salts. 2,4-Dioxothiazolidine-5-acetic acid and different coformers (listed below) under ambient conditions and solvents were used for the synthesis of organic salts.

- Benzimidazole
- 2-Methylbenzimidazole
- Ethylenediamine

Equimolar quantities of 2,4-dioxothiazolidine-5-acetic acid and benzimidazole/ethylenediamine were dissolved separately in a mixture of ethanol and water (5:1), whereas methyl benzimidazole was dissolved in ethanol. Solutions of 2,4-dioxothiazolidine-5-acetic acid and coformers were mixed and warmed up to the temperature of 50 °C for a few minutes and set aside for deliberate evaporation. Brown crystals of salt of 2,4-dioxothiazolidine-5-acetic acid and benzimidazole (**1**) were obtained after 3 days. Colorless prism-like crystals of 2,4-dioxothiazolidine-5-acetic acid and 2-methylbenzimidazole (**2**) were formed after a time span of 8 days, whereas colorless crystals of 2,4-dioxothiazolidine-5-acetic acid and ethylenediamine (**3**) were isolated after 10 days. The crystals were filtrated and dried at room temperature (Scheme 2), and the physical properties of obtained organic salts are presented in Table 1.

Structural Characterization. UV/vis studies were performed using UV-1700 (Shimadzu, Japan), whereas functional group characterization was performed by exposing the sample to IR frequencies in the range of 4000−659 cm^{-1} using a thermoclinical (NICOLET-iS10, Japan) spectrophotometer. This analysis is given in the Supporting Information, and the results are shown in Table S1.

The crystals of suitable quality and size were exposed to a monochromatic X-ray beam using a Bruker Kappa APEX-II CCD diffractometer containing a graphite monochromator at 296 (2) K. Kα X-rays of molybdenum were utilized with fine focus. The APEX-II software was used for data collection, whereas the SADABS software was used for the absorption correction. The SHELXT-2014[51] and SHELXL 2019/2[52] software were used for the structure solution and refinement, respectively. The nonhydrogen atoms were refined by using anisotropic displacement parameters, whereas isotropic displacement parameters were assigned to H-atoms. All the H-atoms were placed at geometrically calculated positions by using the riding model except for the hydrogen atoms of water in compounds **2** and **3**. The hydrogens of water were refined freely for assigning the correction orientations. ORTEP-III,[53] PLATON,[54] and Mercury version 4.0[55] were used for the graphical representations of single-crystal XRD results.

DSC tests were performed to contemplate the thermal conduct of the crystals, and for this purpose, a DTG-60H (Shimadzu, Japan) instrument was used.

Computational Procedure. DFT/TDDFT calculations were carried out by utilizing the Gaussian 09 program package[56] with the M06/6-311G(d,p) basis set to investigate the quantum chemical computations of studied compounds (**1** and **2**). For organizing input files, GaussView 6.0 was used.[57] For further interpretation of results, Chemcraft,[58] GaussSum, ArgusLab,[59] and Avogadro[60] were used. Furthermore, to study optoelectronic properties and the structure−property relationship of entitled molecules, frontier molecular orbital (FMO), absorption spectrum (UV−vis) and natural bond orbital (NBO), natural population, and molecular electrostatic potential (MESP) analyses were examined at the M06 level and 6-311G(d,p) basis set. Frontier molecular orbital (FMO) inspection was performed using the M06/6-311G(d,p) level of DFT, and the energy difference between its orbitals was used to calculate the global reactivity parameters (GRPs). So, evaluation of various global reactivity parameters such as electronegativity (X), softness (σ), hardness (η), and chemical potential (μ) analyses were accomplished employing the above functional. NBO analysis was also accomplished at the mentioned level of theory to estimate the stability of compounds.

Molecular Docking. For molecular docking, the MOE 2015 software package was used. The PDB files of DNA (PDB ID: 1D18) and fungal proteins (PDB ID: 1OSY) were downloaded from the Protein Data Bank and were prepared for molecular docking as already reported.[10] The DNA and

https://doi.org/10.1021/acsomega.3c02895
ACS Omega 2023, 8, 30186−30198

protein molecules were used as rigid receptors toward flexible ligands' merged structures.

The ligand molecules were processed to obtain salt conformations as follows: The structure 2,4-dioxothiazolidine-5-acetic acid was drawn in MOE and was subjected to energy minimization. This was declared as a monomer. The structures of benzimidazole, 2-methylbenzimidazoles, and ethylenediamine were drawn, optimized, and declared as coformers. These conformers were entered in the molecular database and merged with the monomer structure in minimized conformation for developing compound **1**, **2**, and **3** structures. The merged **1**−**3** structures were optimized and used as flexible ligands for binding with rigid receptors. The lowest energy docked conformation were analyzed for interactional investigation.

■ ASSOCIATED CONTENT

Supporting Information

The Supporting Information is available free of charge at https://pubs.acs.org/doi/10.1021/acsomega.3c02895.

UV−vis analysis, comparison of XRD and DFT studies, NPA analysis, MEP analysis, IR spectra, and DSC analysis (overall, there are 17 tables (S1−S17) and 16 figures (S1−S16) included for further elaboration of the text in the manuscript) (PDF)

■ AUTHOR INFORMATION

Corresponding Authors

Moazzam H. Bhatti − *Department of Chemistry, Allama Iqbal Open University, Islamabad 44000, Pakistan;* orcid.org/0000-0003-4868-6032; Email: moazzamhussain_b@yahoo.com

Suvash Chandra Ojha − *Department of Infectious Diseases, The Affiliated Hospital of Southwest Medical University, Luzhou, Sichuan 646000, China*; Email: suvash_ojha@swmu.edu.cn

Authors

Syed Muddassir Ali Mashhadi − *Department of Chemistry, University of Sialkot, Sialkot, Punjab 56400, Pakistan; Department of Chemistry, Allama Iqbal Open University, Islamabad 44000, Pakistan;* orcid.org/0000-0002-6455-7604

Erum Jabeen − *Department of Chemistry, Allama Iqbal Open University, Islamabad 44000, Pakistan*

Uzma Yunus − *Department of Chemistry, Allama Iqbal Open University, Islamabad 44000, Pakistan*

Muhammad Ashfaq − *Department of Physics, University of Sargodha, Sargodha, Punjab 40100, Pakistan;* orcid.org/0000-0001-6663-8777

Mahjbeen Akhtar − *Department of Chemistry, Allama Iqbal Open University, Islamabad 44000, Pakistan*

Muhammad Nawaz Tahir − *Department of Physics, University of Sargodha, Sargodha, Punjab 40100, Pakistan*

Saad M. Alshehri − *Department of Chemistry, College of Science, King Saud University, Riyadh 11451, Saudi Arabia*

Sarfraz Ahmed − *Wellman Center for Photomedicine, Harvard Medical School, Massachusetts General Hospital, Boston, Massachusetts 02114, United States*

Complete contact information is available at: https://pubs.acs.org/10.1021/acsomega.3c02895

Notes

The authors declare no competing financial interest.

■ ACKNOWLEDGMENTS

The authors thank the Researchers Supporting Project (number RSP2023R29), King Saud University, Riyadh, Saudi Arabia. S.C.O. acknowledges the support from the doctoral research fund of the Affiliated Hospital of Southwest Medical University.

■ REFERENCES

(1) Muddassir, S.; Mashhadi, A.; Yunus, U.; Hussain, M.; Nawaz, M. Isoniazid Cocrystals with Anti-Oxidant Hydroxy Benzoic Acids Gallic Acid. *J. Mol. Struct.* **2014**, *1076*, 446−452.

(2) Mashhadi, S. M. A.; Yunus, U.; Bhatti, M. H.; Ahmed, I.; Tahir, M. N. Synthesis, Characterization, Solubility and Stability Studies of Hydrate Cocrystal of Antitubercular Isoniazid with Antioxidant and Anti-Bacterial Protocatechuic Acid. *J. Mol. Struct.* **2016**, *1117*, 17−21.

(3) Lehn, J. M. Toward Self-Organization and Complex Matter. *Science* **2002**, 2400.

(4) Cram, D. J. The Design of Molecular Hosts, Guests, and Their Complexes (Nobel Lecture). *Angew. Chem., Int. Ed. Engl.* **1988**, 1009.

(5) Cruz-Cabeza, A. J.; Lusi, M.; Wheatcroft, H. P.; Bond, A. D. The Role of Solvation in Proton Transfer Reactions: Implications for Predicting Salt/co-Crystal Formation Using the ΔpKa Rule. *Faraday Discuss. Chem. Soc.* **2022**, 446.

(6) Cram, D. J.; Cram, J. M. Design of Complexes between Synthetic Hosts and Organic Guests. *Acc. Chem. Res.* **1978**, 8.

(7) Carvalho, P. S.; Diniz, L. F.; Tenorio, J. C.; Souza, M. S.; Franco, C. H. J.; Rial, R. C.; Warszawski De Oliveira, K. R.; Nazario, C. E. D.; Ellena, J. Pharmaceutical Paroxetine-Based Organic Salts of Carboxylic Acids with Optimized Properties: The Identification and Characterization of Potential Novel API Solid Forms. *CrystEngComm* **2019**, 3668.

(8) Odiase, I.; Nicholson, C. E.; Ahmad, R.; Cooper, J.; Yufit, D. S.; Cooper, S. J. Three Cocrystals and a Cocrystal Salt of Pyrimidin-2-Amine and Glutaric Acid. *Acta Crystallogr., Sect. C: Struct. Chem.* **2015**, *71*, 276−283.

(9) Mashhadi, S. M. A.; Tahir, M. N.; Apperley, D.; Bhatti, M. H.; Ashfaq, M.; Yunus, U. Pharmaceutical Organic Salt: Disordered Crystal Structure of Levofloxacin with γ-Resorcylic Acid. *Eur. J. Chem.* **2021**, *12*, 323.

(10) Wyss, D. F.; Eaton, H. L. Fragment-Based Approaches to Lead Discovery. In *Frontiers in Drug Design & Discovery: Structure-Based Drug Design in the 21st Century*; Bentham Science Publishers, 2007; Vol. *171*, pp. 171−202.

(11) Abd El-Karim, S. S.; Mohamed, H. S.; Abdelhameed, M. F.; Amr, A. E.-G. E.; Almehizia, A. A.; Nossier, E. S. Design, Synthesis and Molecular Docking of New Pyrazole-Thiazolidinones as Potent Anti-Inflammatory and Analgesic Agents with TNF-α Inhibitory Activity. *Bioorg. Chem.* **2021**, *111*, No. 104827.

(12) Havrylyuk, D.; Zimenkovsky, B.; Karpenko, O.; Grellier, P.; Lesyk, R. Synthesis of Pyrazoline-Thiazolidinone Hybrids with Trypanocidal Activity. *Eur. J. Med. Chem.* **2014**, *85*, 245.

(13) Nitsche, C.; Schreier, V. N.; Behnam, M. A. M.; Kumar, A.; Bartenschlager, R.; Klein, C. D. Thiazolidinone-Peptide Hybrids as Dengue Virus Protease Inhibitors with Antiviral Activity in Cell Culture. *J. Med. Chem.* **2013**, *56*, 8389.

(14) Patel, N. B.; Patel, M. D. Synthesis and Evaluation of Antibacterial and Antifungal Activities of 4-Thiazolidinones and 2-Azetidinones Derivatives from Chalcone. *Med. Chem. Res.* **2017**, *26*, 1772.

(15) Iqbal, M. A.; Husain, A.; Alam, O.; Khan, S. A.; Ahmad, A.; Haider, M. R.; Alam, M. A. Design, Synthesis, and Biological Evaluation of Imidazopyridine-Linked Thiazolidinone as Potential Anticancer Agents. *Arch. Pharm. (Weinheim)* **2020**, *353*, No. 2000071.

(16) Camacho, J.; Barazarte, A.; Gamboa, N.; Rodrigues, J.; Rojas, R.; Vaisberg, A.; Gilman, R.; Charris, J. Synthesis and Biological

Evaluation of Benzimidazole-5-Carbohydrazide Derivatives as Antimalarial, Cytotoxic and Antitubercular Agents. *Bioorg. Med. Chem.* **2011**, *19*, 2023.
(17) Singh, S. P.; Parmar, S. S.; Raman, K.; Stenberg, V. I. Chemistry and Biological Activity of Thiazolidinones. *Chem. Rev.* **1981**, *81*, 175.
(18) Bhatti, R. S.; Shah, S.; Suresh; Krishan, P.; Sandhu, J. S. Recent Pharmacological Developments on Rhodanines and 2,4-Thiazolidinediones. *Int. J. Med. Chem.* **2013**, *2013*, 1.
(19) Sawant, R. L.; Wadekar, J. B.; Kharat, S. B.; Makasare, H. S. Targeting PPAR-γ to Design and Synthesize Antidiabetic Thiazolidines. *EXCLI J.* **2018**, *17*, 598.
(20) Gajić, M.; Džambaski, Z.; Ilić, B. S.; Kocić, G.; Bondžić, B. P.; Šmelcerović, A. Synthesis and Analysis of 4-Oxothiazolidines as Potential Dual Inhibitors of Deoxyribonuclease I and Xanthine Oxidase. *Chem.-Biol. Interact.* **2021**, *345*, No. 109536.
(21) Meng, X.-Y.; Zhang, H.-X.; Mezei, M.; Cui, M. Molecular Docking: A Powerful Approach for Structure-Based Drug Discovery. *Curr. Comput.-Aided Drug Des.* **2011**, *7*, 146.
(22) Ramsay, R. R.; Popovic-Nikolic, M. R.; Nikolic, K.; Uliassi, E.; Bolognesi, M. L. A Perspective on Multi-target Drug Discovery and Design for Complex Diseases. *Clin. Transl. Med.* **2018**, *7*, 3.
(23) Spackman, P. R.; Turner, M. J.; McKinnon, J. J.; Wolff, S. K.; Grimwood, D. J.; Jayatilaka, D.; Spackman, M. A. CrystalExplorer: A Program for Hirshfeld Surface Analysis, Visualization and Quantitative Analysis of Molecular Crystals. *J. Appl. Crystallogr.* **2021**, *54*, 1006.
(24) Ashfaq, M.; Nawaz Tahir, M.; Munawar, K. S.; Behjatmanesh-Ardakani, R.; Kargar, H. Single Crystal Exploration, Supramolecular Behaviour, Hirshfeld Surface Analysis, Linear and Non-Linear Theoretical Optical Properties of Schiff Bases Derived from Benzene Sulfonamides. *J. Mol. Struct.* **2022**, *1261*, No. 132952.
(25) Malik, A. N.; Kuznetsov, A.; Ali, A.; Ashfaq, M.; Tahir, M. N.; Siddique, A. Imine-Based Zwitterion: Synthesis, Single-Crystal Characterization, and Computational Investigation. *J. Mol. Struct.* **2022**, *1253*, No. 132237.
(26) Muthu, S.; Maheswari, J. U. Quantum Mechanical Study and Spectroscopic (FT-IR, FT-Raman, ^{13}C, ^{1}H, UV) Study, First Order Hyperpolarizability, NBO Analysis, HOMO and LUMO Analysis of 4-[(4-Aminobenzene) Sulfonyl] Aniline by Ab Initio HF and Density Functional Method. *Spectrochim. Acta, Part A* **2012**, *92*, 154.
(27) Foster, J. P.; Weinhold, F. Natural Hybrid Orbitals. *J. Am. Chem. Soc.* **1980**, *102*, 7211.
(28) Khan, M. U.; Iqbal, J.; Khalid, M.; Hussain, R.; Braga, A. A. C.; Hussain, M.; Muhammad, S. Designing Triazatruxene-Based Donor Materials with Promising Photovoltaic Parameters for Organic Solar Cells. *RSC Adv.* **2019**, *9*, 26402.
(29) Khalid, M.; Khan, M. U.; Azhar, N.; Arshad, M. N.; Asiri, A. M.; Braga, A. A. C.; Akhtar, M. N. Exploration of Nonlinear Optical Enhancement and Interesting Optical Behavior with Pyrene Moiety as the Conjugated Donor and Efficient Modification in Acceptor Moieties. *Opt. Quantum Electron.* **2022**, *54*, 395.
(30) Khalid, M.; Khan, M. U.; Razia, E.; Shafiq, Z.; Alam, M. M.; Imran, M.; Akram, M. S. Exploration of Efficient Electron Acceptors for Organic Solar Cells: Rational Design of Indacenodithiophene Based Non-Fullerene Compounds. *Sci. Rep.* **2021**, *11*, 19931.
(31) Khan, M. U.; Ibrahim, M.; Khalid, M.; Qureshi, M. S.; Gulzar, T.; Zia, K. M.; Al-Saadi, A. A.; Janjua, M. R. S. A. First Theoretical Probe for Efficient Enhancement of Nonlinear Optical Properties of Quinacridone Based Compounds through Various Modifications. *Chem. Phys. Lett.* **2019**, *715*, 222.
(32) Janjua, M. R. S. A.; Khan, M. U.; Bashir, B.; Iqbal, M. A.; Song, Y.; Naqvi, S. A. R.; Khan, Z. A. Effect of π-Conjugation Spacer (CC) on the First Hyperpolarizabilities of Polymeric Chain Containing Polyoxometalate Cluster as a Side-Chain Pendant: A DFT Study. *Comput. Theor. Chem.* **2012**, *994*, 34.
(33) Khalid, M.; Khan, M. U.; Ahmed, S.; Shafiq, Z.; Alam, M. M.; Imran, M.; Braga, A. A. C.; Akram, M. S. Exploration of Promising Optical and Electronic Properties of (Non-Polymer) Small Donor Molecules for Organic Solar Cells. *Sci. Rep.* **2021**, *11*, 21540.
(34) Khalid, M.; Anwer, W.; Adeel, M.; Shafiq, Z.; Braga, A. A. C.; Assiri, M. A.; Imran, M.; Ullah, A. Exploration of the Interesting Photovoltaic Behavior of the Fused Benzothiophene Dioxide Moiety as a Core Donor with Modification in Acceptors for High-Efficacy Organic Solar Cells. *RSC Adv.* **2022**, *12*, 29010−29021.
(35) Fonseca, R. D.; Vivas, M. G.; Silva, D. L.; Eucat, G.; Bretonnière, Y.; Andraud, C.; De Boni, L.; Mendonça, C. R. First-Order Hyperpolarizability of Triphenylamine Derivatives Containing Cyanopyridine: Molecular Branching Effect. *J. Phys. Chem. C* **2018**, *122*, 1770.
(36) Khalid, M.; Shafiq, I.; Zhu, M.; Khan, M. U.; Shafiq, Z.; Iqbal, J.; Alam, M. M.; Braga, A. A. C.; Imran, M. Efficient Tuning of Small Acceptor Chromophores with A1-π-A2-π-A1 Configuration for High Efficacy of Organic Solar Cells via End Group Manipulation. *J. Saudi Chem. Soc.* **2021**, *25*, No. 101305.
(37) Khalid, M.; Shafiq, I.; Ahmed, R.; Arshad, M.; Asghar, M. A.; Munawar, K. S.; Imran, M.; Braga, A. A. C. First Theoretical Framework for Highly Efficient Photovoltaic Parameters by Structural Modification with Benzothiophene-Incorporated Acceptors in Dithiophene Based Chromophores. *Sci. Rep.* **2022**, *12*, 20148.
(38) Janjua, M. R. S. A.; Khan, M. U.; Khalid, M.; Ullah, N.; Kalgaonkar, R.; Alnoaimi, K.; Baqader, N.; Jamil, S. Theoretical and Conceptual Framework to Design Efficient Dye-Sensitized Solar Cells (DSSCs): Molecular Engineering by DFT Method. *J. Cluster Sci.* **2021**, *32*, 243−253.
(39) Asad, M.; Arshad, M. N.; Oves, M.; Khalid, M.; Khan, S. A.; Asiri, A. M.; Rehan, M.; Dzudzevic-Cancar, H. N-Trifluoroacetylated Pyrazolines: Synthesis, Characterization and Antimicrobial Studies. *Bioorg. Chem.* **2020**, *99*, No. 103842.
(40) Akram, M.; Adeel, M.; Khalid, M.; Tahir, M. N.; Aliabad, H. A. R.; Ullah, M. A.; Iqbal, J.; Braga, A. A. C. Highly Efficient One Pot Palladium-Catalyzed Synthesis of 3, 5-Bis (Arylated) Pyridines: Comparative Experimental and DFT Studies. *J. Mol. Struct.* **2020**, *1213*, No. 128131.
(41) Khalid, M.; Naz, S.; Mahmood, K.; Hussain, S.; Braga, A. A. C.; Hussain, R.; Ragab, A. H.; Al-Mhyawi, S. R. First Theoretical Probe for Efficient Enhancement of Optical Nonlinearity via Structural Modifications into Phenylene Based D−π−A Configured Molecules. *RSC Adv.* **2022**, *12*, 31192−31204.
(42) Zhai, D.; Ma, C.; Ma, P.; Pan, Y.; Hao, L.; Liu, X.; Jiang, J. Theoretical Insight into Different Energetic Groups on the Performance of Energetic Materials Featuring RDX Ring. *Fuel* **2021**, *294*, No. 120497.
(43) Hao, L.; Liu, X.; Zhai, D.; Qiu, L.; Ma, C.; Ma, P.; Jiang, J. Theoretical Studies on the Performance of HMX with Different Energetic Groups. *ACS Omega* **2020**, *5*, 29922−29934.
(44) Ma, P.; Xu, X.; Zhang, R.; Ma, C.; Liu, X.; Hao, L.; Pan, Y.; Jiang, J. Synthesis, Thermal Hazard Analysis and Density Functional Theory Study of Nitroimidazoles. *Thermochim. Acta* **2022**, *707*, No. 179097.
(45) Xu, X.; Zhang, R.; Xia, W.; Ma, P.; Ma, C.; Pan, Y.; Jiang, J. Density Functional Theory Study of CL-20/Nitroimidazoles Energetic Cocrystals in an External Electric Field. *Comput. Theor. Chem.* **2022**, *1209*, No. 113607.
(46) Okulik, N.; Jubert, A. H. Theoretical Analysis of the Reactive Sites of Non−steroidal Anti−inflammatory Drugs. *Internet Electron. J. Mol. Des.* **2005**, *4*, 17.
(47) Bradshaw, W. J.; Bruxelle, J. F.; Kovacs-Simon, A.; Harmer, N. J.; Janoir, C.; Péchiné, S.; Acharya, K. R.; Michell, S. L. Molecular Features of Lipoprotein CD0873: A Potential Vaccine against the Human Pathogen Clostridioides Difficile. *J. Biol. Chem.* **2019**, *294*, 15850.
(48) Jabeen, T.; Singh, N.; Singh, R. K.; Sharma, S.; Somvanshi, R. K.; Dey, S.; Singh, T. P. Non-Steroidal Anti-Inflammatory Drugs as Potent Inhibitors of Phospholipase A2: Structure of the Complex of Phospholipase A2 with Niflumic Acid at 2.5 Å Resolution. *Acta Crystallogr., Sect. D: Biol. Crystallogr.* **2005**, *61*, 1579.
(49) Kutin, Y.; Kositzki, R.; Branca, R. M. M.; Srinivas, V.; Lundin, D.; Haumann, M.; Högbom, M.; Cox, N.; Griese, J. J. Chemical

https://doi.org/10.1021/acsomega.3c02895
ACS Omega 2023, 8, 30186−30198

Flexibility of Heterobimetallic Mn/Fe Cofactors: R2lox and R2c Proteins. *J. Biol. Chem.* **2019**, *294*, 18372.
(50) Zimenkovskii, B. S.; Kutsyk, R. V.; Lesyk, R. B.; Matyichuk, V. S.; Obushak, N. D.; Klyufinska, T. I. Synthesis and Antimicrobial Activity of 2,4-Dioxothiazolidine-5-Acetic Acid Amides. *Pharm. Chem. J.* **2006**, *40*, 303.
(51) Sheldrick, G. M. SHELXT - Integrated Space-Group and Crystal-Structure Determination. *Acta Crystallogr., Sect. A: Found. Crystallogr.* **2015**, 3.
(52) Sheldrick, G. M. Crystal Structure Refinement with SHELXL. *Acta Crystallogr., Sect. C: Struct. Chem.* **2015**, *71*, 3−8.
(53) Farrugia, L. J. WinGX and ORTEP for Windows: An Update. *J. Appl. Crystallogr.* **2012**, *45*, 849−854.
(54) Spek, A. L. Structure Validation in Chemical Crystallography. *Acta Crystallogr., Sect. D: Struct. Biol.* **2009**, *65*, 148−155.
(55) Macrae, C. F.; Sovago, I.; Cottrell, S. J.; Galek, P. T. A.; McCabe, P.; Pidcock, E.; Platings, M.; Shields, G. P.; Stevens, J. S.; Towler, M.; Wood, P. A. Mercury 4.0: From Visualization to Analysis, Design and Prediction. *J. Appl. Crystallogr.* **2020**, *53*, 226−235.
(56) Frisch, M. J.; Trucks, G. W.; Schlegel, H. B.; Scuseria, G. E.; Robb, M. A.; Cheeseman, J. R.; Scalmani, G.; Barone, V.; Mennucci, B.; Petersson, G. A.; Nakatsuji, H.; Caricato, M.; Li, X.; Hratchian, H. P.; Izmaylov, A. F.; Bloino, J.; Zheng, G.; Sonnenberg; Hada, J. L. J. F. D. *Gaussian 09, Revision A. 02*; Gaussian, Inc.: Wallingford, CT, 2009 *1988*, 37.
(57) Dennington, R.; Keith, T. A.; Millam, J. M. *GaussView, Version 6.0. 16; GaussView, Version 6*; Semichem Inc. Shawnee Mission KS, 2016.
(58) Zhurko, G. A.; Zhurko, D. A. ChemCraft-Graphical Program for Visualization of Quantum Chemistry Computations. *Chemcr. v1.8*; 2020.
(59) Thompson, M. A. Molecular Docking Using ArgusLab, an Efficient Shape-Based Search Algorithm and the AScore Scoring Function. In *ACS Meeting*; 2004.
(60) Hanwell, M. D.; Curtis, D. E.; Lonie, D. C.; Vandermeerschd, T.; Zurek, E.; Hutchison, G. R. Avogadro: An Advanced Semantic Chemical Editor, Visualization, and Analysis Platform. *J. Cheminform.* **2012**, *4*, 17.

https://doi.org/10.1021/acsomega.3c02895
ACS Omega 2023, 8, 30186−30198